

Influence of temperature on power factor and operating area of SynRM machine in automotive equipment

Mohd Azri Hizami Rasid¹, Vincent Lanfranchi², Alejandro Ospina², Khadija Benkara²

¹Faculty of Manufacturing and Mechatronics Engineering Technology, Universiti Malaysia Pahang Al-Sultan Abdullah (UMPSA), Pekan, Malaysia

²FRE UTC-CNRS 2012, Laboratoire Roberval, Sorbonne University, Université de Technologie de Compiègne, Compiègne, France

Article Info

Article history:

Received May 4, 2023

Revised Jul 22, 2023

Accepted Aug 9, 2023

Keywords:

Automotive

Power factor

SynRM

Temperature

Torque speed operating area

ABSTRACT

Across various applications, electrical machines are intensely replacing conventional hydraulic and pneumatic actuators in applications with a higher degree of complexity. In our previous study, a SynRM machine with a segmented rotor was designed to operate as a clutch actuator, to be placed in the gear housing which suffers from a high ambient temperature. This makes it necessary to predict the considerable potential influence of temperatures. This study evaluates the influence of winding resistance variation due to temperature on the machine power factor and its operating area. The evaluation is done for the condition of the automotive battery supply of 14 V, 50 A. An experimentally validated analytical model based on the SynRM machine phasor diagram was used to assess the torque-speed area and power factor variation. The main contribution is presented in the form of a tool represented as an abacus that allows the user of the machine to track the power factor and maximum speed for a range of winding resistance values. On a selected operating point of $(\Gamma, N) = (0.57 \text{ N.m}, 3500 \text{ rpm})$, it is demonstrated that the winding resistance should be reduced below 0.2Ω , to be able to achieve the targeted speed, while the power factor is at 0.9.

This is an open access article under the [CC BY-SA](https://creativecommons.org/licenses/by-sa/4.0/) license.



Corresponding Author:

Mohd Azri Hizami Rasid

Faculty of Manufacturing and Mechatronics Engineering Technology,

Universiti Malaysia Pahang Al-Sultan Abdullah (UMPSA)

26600 Pekan, Pahang, Malaysia

Email: mahizami@ump.edu.my

1. INTRODUCTION

Besides being used for the main traction motor development, the integration of motors into other major functions of an automobile have seen many phases of improvement and optimization [1]–[3]. In our study previously presented in [4]–[6], a synchronous reluctance machine (SynRM) machine was designed to operate as a clutch actuator, and placed inside the gear housing. The ambient temperature can reach up to $140 \text{ }^\circ\text{C}$. The segmented rotor SynRM topology was chosen. The advantages of this topology of SynRM are that it is void of permanent magnets and the rotor is easy to fabricate for a small-size rotor [7]. A more popular flux barrier SynRM [8] is here irrelevant due to the manufacturing difficulties of stamping a small flux barrier in the rotor, and the high possibility of having saturation around the barrier. The design, dimensions, and assembly of the prototype can be found in the Figures 1 and 2. Figures 1 and 2 show the design, dimensions, and assembly of the SynRM prototype machine. The maximum torque load angle is at $\beta = 45^\circ$.

Studies regarding its thermal behavior and losses were extensively done to ensure that the machine can cope with the load without damaging its winding insulation [6], [9] which is the only thermal-sensitive component in the machine. Tested for the WLTP speed profile, the clutch application shows that the SynRM

temperature stays within the safe temperature range. Now that we are sure that the machine will not be damaged by the temperature, it is necessary to evaluate the consequence of the temperature on the electromechanical performance of the machine, namely the torque-speed operating area and power factor.

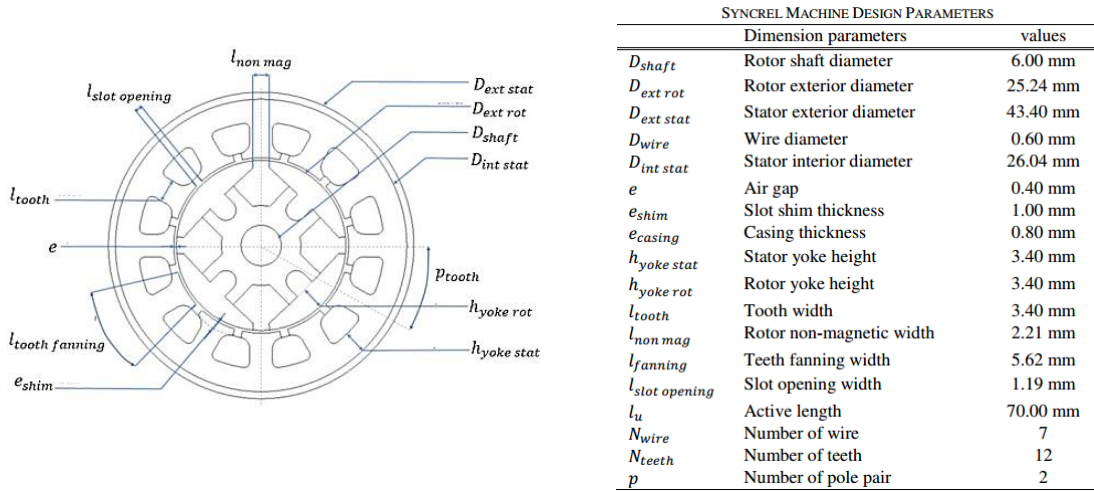


Figure 1. Design and dimensions of the SynRM prototype machine

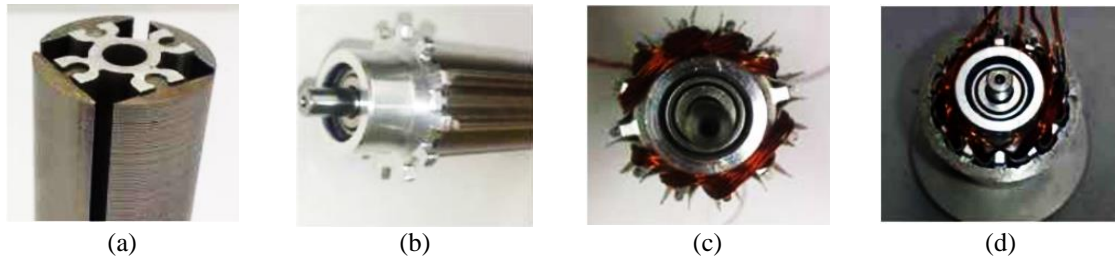


Figure 2. The assembly of the SynRM with a segmented rotor machine: (a) complete mounted rotor, (b) mounting the teeth on the bearing housing, (c) complete winding on the already mounted teeth, and (d) completed Syncrel motor assembly

For power factor, it is important to evaluate it to estimate the efficiency and properly design the power electronics components [10], [11]. It has been established in multiple studies, that the low power factor of a SynRM machine is a natural limitation due to the saliency [12]–[14]. It has also been demonstrated that having a high-power factor and a high efficiency at the same time may be conflicting objectives. As an example, in [12], the choice of design has to be made by balancing the compromise between power factor and efficiency (Figure 3). A higher power factor design may lead to a lower efficiency, therefore a higher badness indicator.

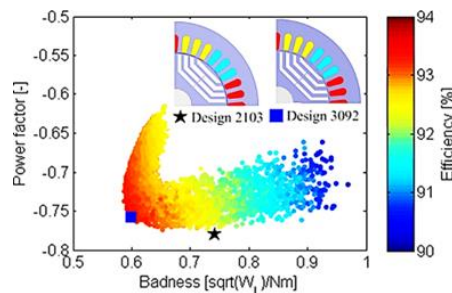


Figure 3. The scatter plot relating the power factor and efficiency following a design optimization to find the best design of a SynRM machine by [12]

The operating area is also important to be reevaluated to make sure that the targeted operating points required by the application are still attainable despite the temperature variation. [15]–[17] for example, have shown the importance of the thermal effects to be properly included in a system performance study. This is valid in different perspectives including for a performance prediction or state-observer and optimum control. Furthermore, in a magnetless SynRM machine, the consequence may be less obvious compared to a permanent-magnet motor, has been studied in different literature such as [18]–[20]. Despite being relatively common knowledge as shown in several references cited, this study's contribution will be specifically in identifying the operating area and power factor variation for the SynRM with the segmented rotor, in an automotive equipment application.

In the following section, a methodology section will explain how the resistance variation due to temperature will be computed, then integrated into a validated analytical model that will output the power factor and torque-speed operating area. Then, the results section will present the variation of torque-speed range and power factor depending on the winding resistance variation. A tool presented in the form of abacus shows the relevance of the study where examples of non-attainable operating points due to resistance increase (temperature increase) will be presented.

2. METHODOLOGY

To evaluate the influence of temperature on the torque-speed operating area and power factor, a validated analytical tools was developed, validated and then used. In this section we will start with detailing how the temperature variation is taken into account as a variation of resistance. Then the details on the development of the analytical model, followed by the validation experiments are presented.

2.1. Winding resistance variation in relation to temperature variation

In our magnetless SynRM, the component that is sensitive and can change behavior with the temperature is winding. Its resistance is temperature dependent. The DC resistance of the copper wire increases with increasing temperature by (1) [21]:

$$R_T = R_0[1 + \alpha(T - T_{20})] \quad (1)$$

Where for a copper conductor, R_T is the resistance of copper at temperature T , R_0 is the resistance of copper at 20 °C (T_{20}), and α is the temperature correction coefficient of copper which is equal to 0.00393/°C. As the temperature increases, the winding resistance will also increase proportionally. Therefore, throughout this article, the influence of the temperature is reflected by the variation of the winding resistance. The initial value of the winding resistance at 20 °C is reported to be at 0.22 Ω [4]. Figure 4(a) shows the rise of winding resistance as the temperature increases. It is known that as a consequence, the copper losses in the machine also increase with temperature. Figure 4(b) shows the variation of the copper losses at the different operating current levels as the temperature varies in the range of 20–200 °C. On the other hand, the variation of power factor and operating area are not as self-evident, which this study tries to answer. This paper will be divided into two sections: The first explains the implementation of an analytical model to compute the power factor and operating area complete with its validation. After that, a section will present the observation and analysis of the results.

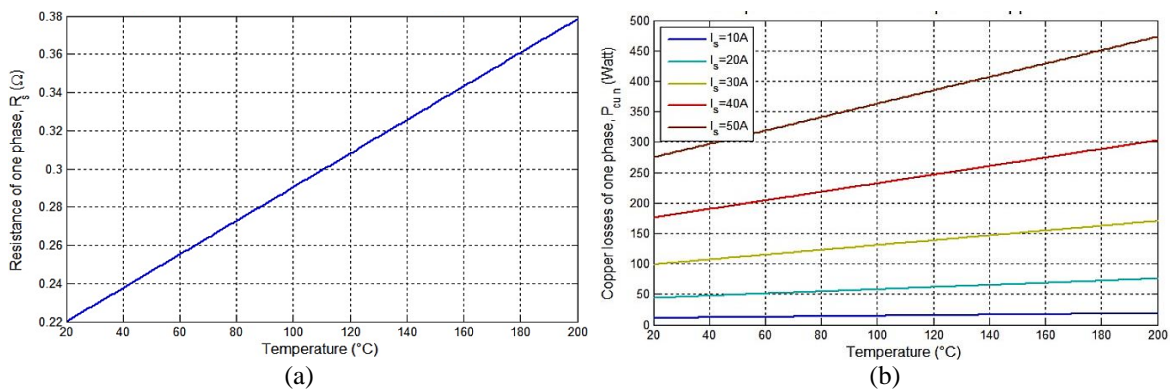


Figure 4. Influence of temperature on (a) SynRM winding resistance and (b) copper losses at different operating currents

2.2. Development of the analytical model for torque-speed operating area and power factor

Deduced from an equivalent circuit, a phasor diagram with properly evaluated parameters can be a versatile tool to evaluate the electromechanical performance of an electrical machine without using any costly numerical tools. The SynRM machine phasor diagram allows us to evaluate different parameters depending on the available input [22]. A tool for fast evaluation of the electromechanical performance using the phasor diagram was developed and presented in [23]. The tools take as input the inductances and the resistance value, then compute the torque-speed operating area using an algorithm that can be described as in Figure 5.

To use the phasor diagram, the inductances were deduced previously using the reluctance network model, and validated by FEA [4], [24]. The machine was designed so that minimum saturation only occurred at the maximum current, therefore the inductances were considered constant. The voltage and current will be swept across a range up to 14 V/50 A which corresponds to an automotive battery's maximum voltage and current. The resistance is the variable that we are going to manipulate as input. The output that we are going to evaluate is first, the torque-speed operating area, and then the power factor $\cos(\phi)$.

For a given power supply (I, V), and a load angle control (β), set of equations from the phasor diagram helps in deducing the speed envelope, power factor, and efficiency. In (2) relates the current with the torque produced while in (3) relates the voltages with the speed [25]. Finally, the power factor can be deduced from the phasor diagram by evaluating the angle between the voltage and current in (4). The computation of the torque-speed operating area and the power factor are then validated experimentally.

$$\Gamma = \frac{3}{4}p(L_d - L_q)I_s^2 \sin 2\beta \tag{2}$$

$$V_s = \sqrt{(R_s I_d - \omega_{elec} L_q I_q)^2 + (R_s I_q - \omega_{elec} L_d I_d)^2} \tag{3}$$

$$\cos\phi = \frac{I_s \cdot V_s}{\dots} \tag{4}$$

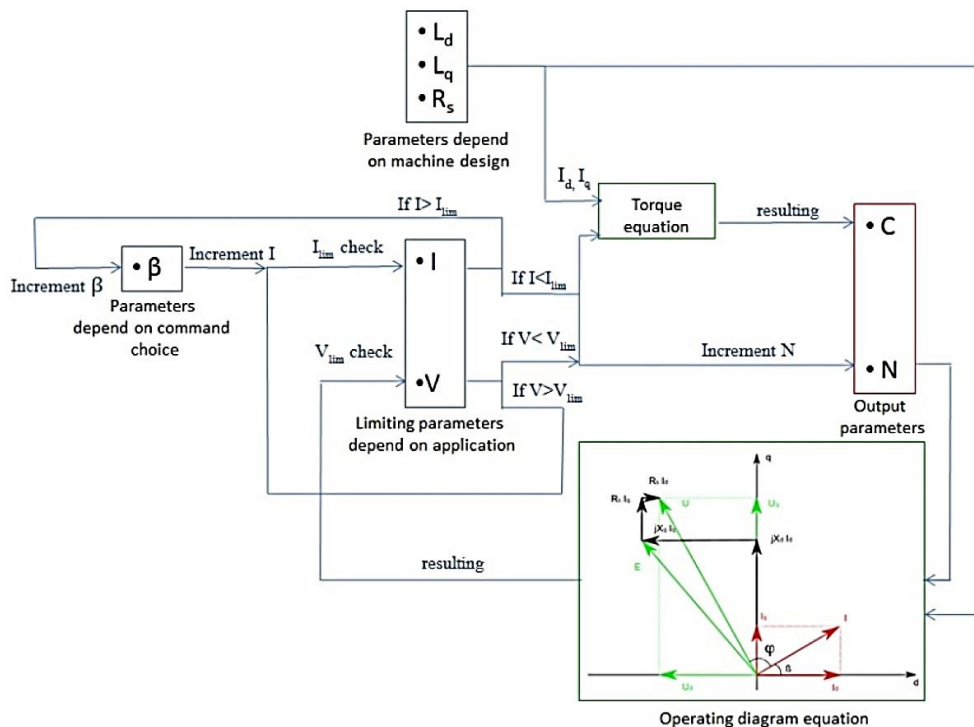


Figure 5. The flow chart of the algorithm used for the construction of the torque-speed area and deduction of power factor using the phasor diagram [23]

2.3. Experimental validation of the analytical model

The prototype machine was mounted on a test bench as shown in Figure 6. The bench is controlled by a Dspace Micro-AutoBox with a command built in Simulink. It is integrated with a Rapid-Pro power unit module for power electronics, integrated with voltage measurement and shunt for current measurement. All

the parameters managed by Micro-Autobox are observable from a host PC and are recorded for post-treatment. The motor is equipped with an incremental encoder with 500 points of resolution. A hysteresis brake serves as load and a torque sensor is used to capture the dynamic torque.

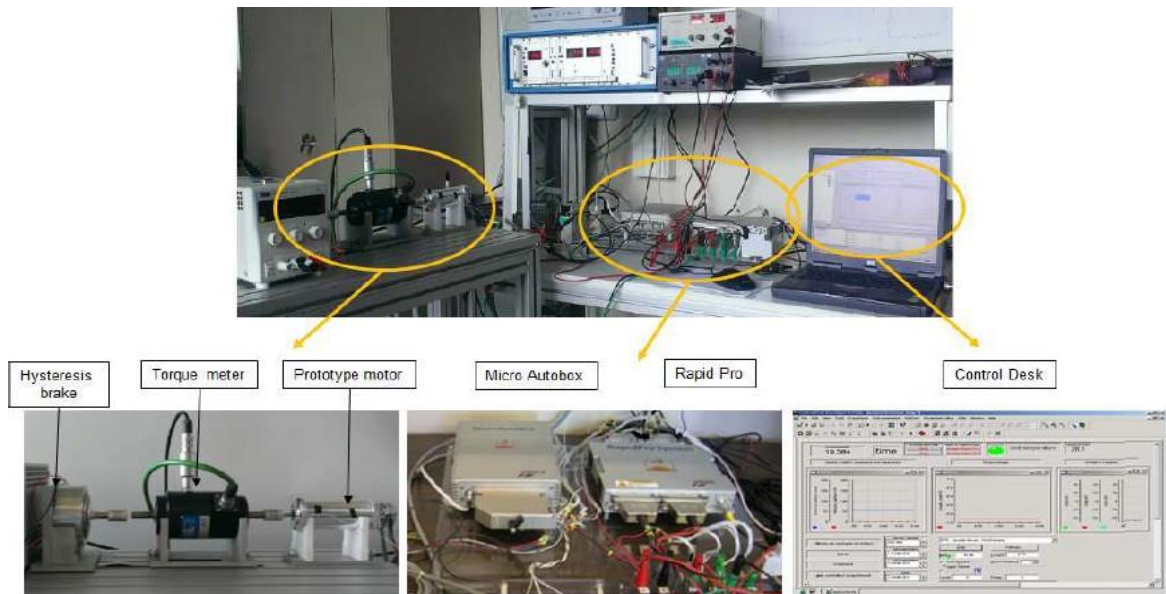


Figure 6. The SynRM test bench

Several operating points of the machine were tested by operating the machine to a constant speed and applying a load (Γ_{exp}). This is done by controlling the machine using speed control and applying load braking. The resulting current and voltage from operating the machine experimentally at (Γ_{exp} , N_{exp}) were then injected into the computation tool to validate the computed torque and speed (Γ_{comp} , N_{comp}). Figure 7 shows the experimental and computed torque Figure 7(a) and speed Figure 7(b) comparison. The coherence of experimental and computer operating points validates the tools for operating area computation.

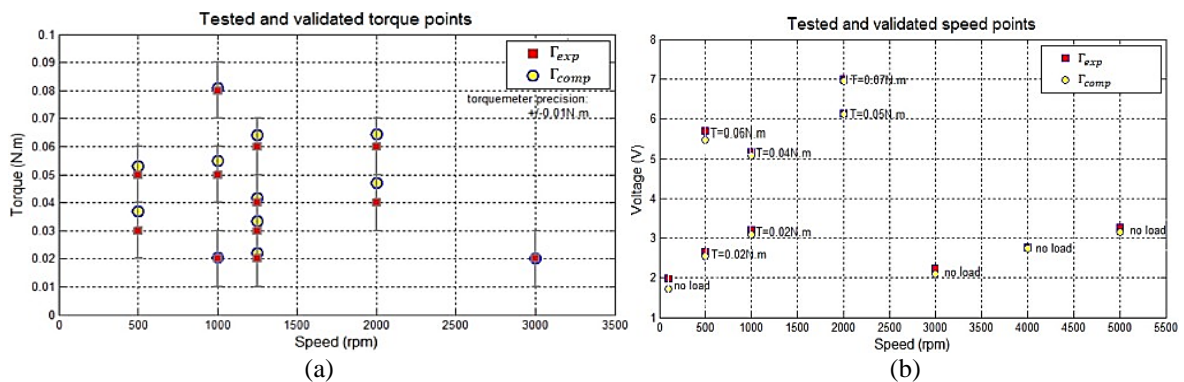


Figure 7. Operating point validation at equal current and voltage for both computation and experiments for: (a) torque and (b) speed

The next performance criteria computation to be validated is the power factor $\cos\phi$. At a given load angle (here $\beta = 45^\circ$, which is the maximum-torque load angle), by maintaining the motor at a constant speed using a speed control at no load, the current and voltage on a winding phase were recorded. The experimental phase shift at different steady-state speeds was later calculated and compared to the computed power factor (Figure 8). Comparison between experimental and computed power factors for speeds ranging from 500 rpm to 5000 rpm shows that the computation tool gives a correct trend and is robust with maximum error on the

power factor of less than 0.05 (Table 1). Having validated the analytical tools for the computation of torque-speed operating area and power factor, the influence of resistance variation (image of temperature variation) on the torque-speed operating area and the power factor can be assessed. This will be presented in the results and analysis section.

Table 1. Computed and experimental $\cos \phi$ comparison

Speed (rpm)	Experimental $\cos \phi$	Computed $\cos \phi$	Error
500	0.97	0.99	0.03
1000	0.95	0.98	0.03
2000	0.91	0.95	0.04
3000	0.87	0.91	0.04

3. RESULTS AND ANALYSIS

We have seen in the introduction that the increase in temperature is reflected in the increase in the winding resistance. All the results presented in the results section are a function of resistance variation, which is an image of a potential temperature variation presented in Figure 4 Here. There are 2 significant findings presented: The reduction of the torque-speed operating area (section 3.1) and the increase of power factor due to increasing temperature. Following these findings, a tool of maximum speed and power factor tracking as a function of winding resistance (which depends on temperature) is developed and presented in section 3.3.

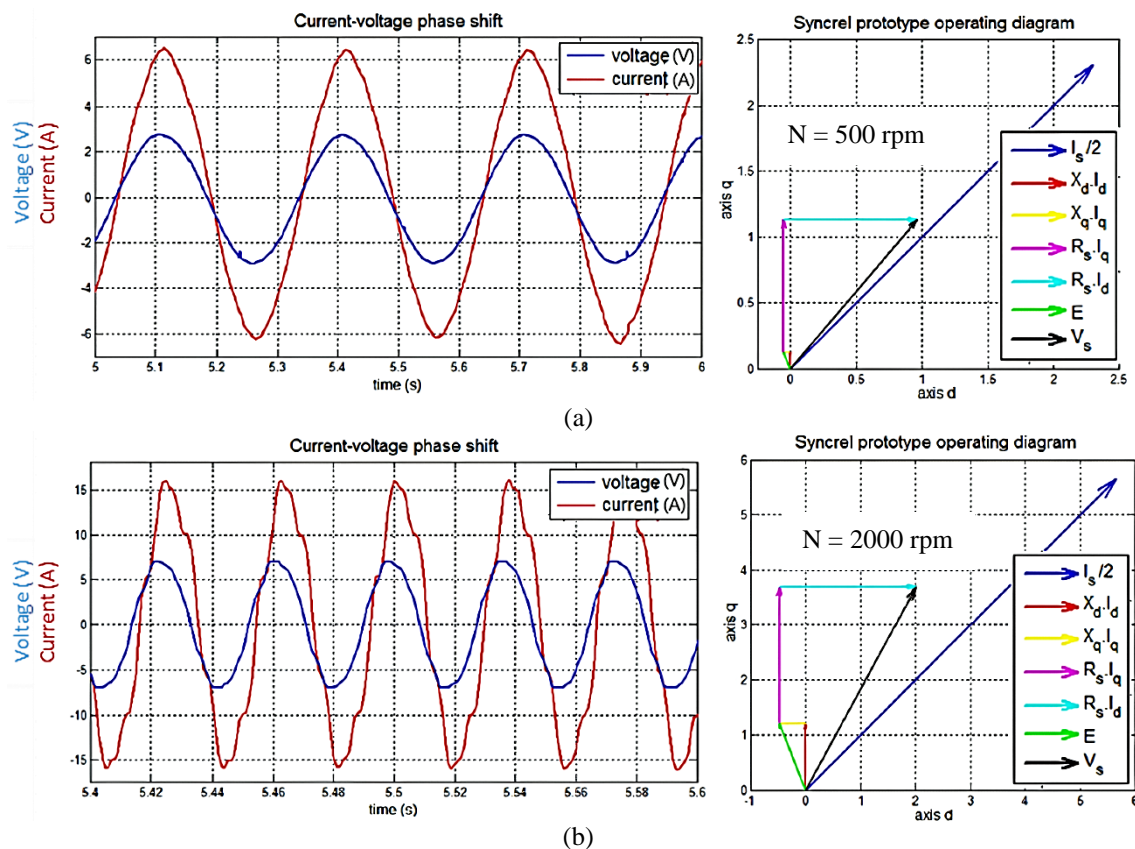


Figure 8. Experimental current-voltage phase shift observed and the corresponding computed operating diagram at: (a) $N = 500$ rpm and (b) $N = 2000$ rpm. ϕ is the angle between the current (blue vector) and the voltage (black vector)

3.1. Reduction of torque-speed operating area due to temperature

Using in (1) and (2) that was implemented in the computation tool, the torque-speed operating area can be plotted following variation of the value of resistance. Figure 9 shows the torque-speed operating area

of the machine plotted for different values of winding resistance ranging from 0.05 to 0.25 Ω which are potential values of our winding resistance. It is shown that as the resistance increases, at a fixed current (torque) level, the maximum speed attainable is reduced. At higher torque, the reduction is more important compared to the one at a low torque point, and the reduction percentage is increasing quadratically due to the sum of the square of the speed in (2) previously shown. This means that due to copper losses, the power output is limited, and this is reflected in the reduction of the maximum speed attainable.

The reduction of the maximum speed means that certain operating points at maximum power on the edge of the operating area envelope may not be attainable at higher temperatures. For example, at 60 $^{\circ}\text{C}$, our winding resistance will be increased up to more than 0.25 Ω , and this will prevent us from attaining the operating point of (0.5 N.m, 5000 rpm).

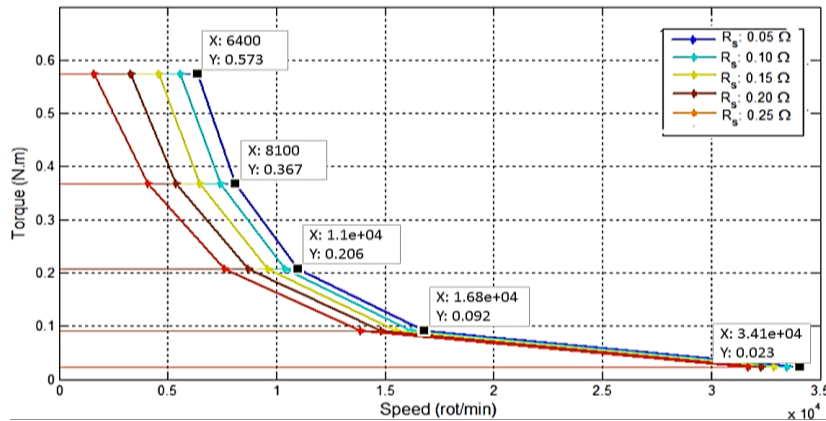


Figure 9. Variation of the operating area as a function of winding resistance R_s for a power supply limited to (50 A, 14 V)

3.2. Power factor increase due to temperature

The power factor is known to be directly related to the speed and load angle of the machine by looking at its phasor diagram. Figure 10 shows the power factor of the SynRM machine plotted against the load angle for different speeds ranging from 1000 to 6000 rpm, which is the operating speed of our application. From the graph, we can see that the increase in speed would decrease the power factor across the machine operating points. On the other hand, the increase in load angle tends to increase the power factor up to a certain maximum point. For our SynRM prototype machine, that angle is at $\beta = 75^{\circ}$.

Additional to the influence of load angle and speed on the power factor, there is also the variation of power factor due to the increase in temperature. Figure 11 shows the variation of power factor as the winding resistance increases at different operating speeds. Unlike the operating area, the increase in winding resistance has increased the power factor. This is explained by the higher resistance terms compared to the inductance terms in (3), which reduce the reactive power by consequence.

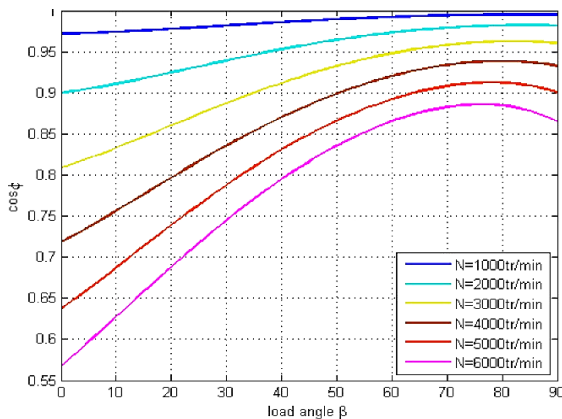


Figure 10. Evolution of $\cos(\phi)$ as a function of load angle β at different speeds

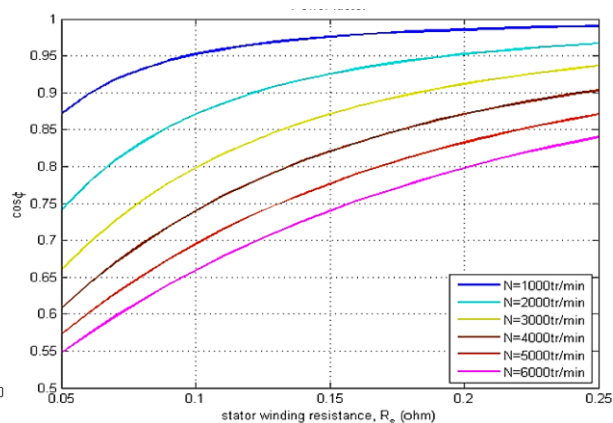


Figure 11. Evolution of $\cos\phi$ as a function of R_s at different speeds

This behavior confirms the findings in the literature such as in [10]–[12] the power factor handicap of operating at higher speed is therefore compensated when the winding resistance is higher. As an example, the power factor of the machine with a resistance of 0.05Ω operating at 6000 rpm can be increased from 0.55 up to 0.84 if the resistance is increased to 0.25Ω . The increase of 0.29 in power factor is certainly consequent in terms of power electronics components and may lead to a potential increase in efficiency. For comparison, with a resistance of 0.05Ω , the same power factor (0.84) can only be achieved if the machine operates at a maximum speed of 1100 rpm (between blue and cyan lines). It is nonetheless an arguable choice to sacrifice in terms of losses by adding the copper losses, which need to be evaluated properly in future studies.

3.3. Tools: abacus for tracking maximum speed and power factor

In previous sections, it has been shown that the maximum speed attainable and the power factor are affected by the increase of temperature through the increase of the winding resistance. To help designers to track the potential degradation of speed and increase of power factor as a function of winding resistance, an abacus combining the results previously presented was built. Figure 12 shows the abacus.

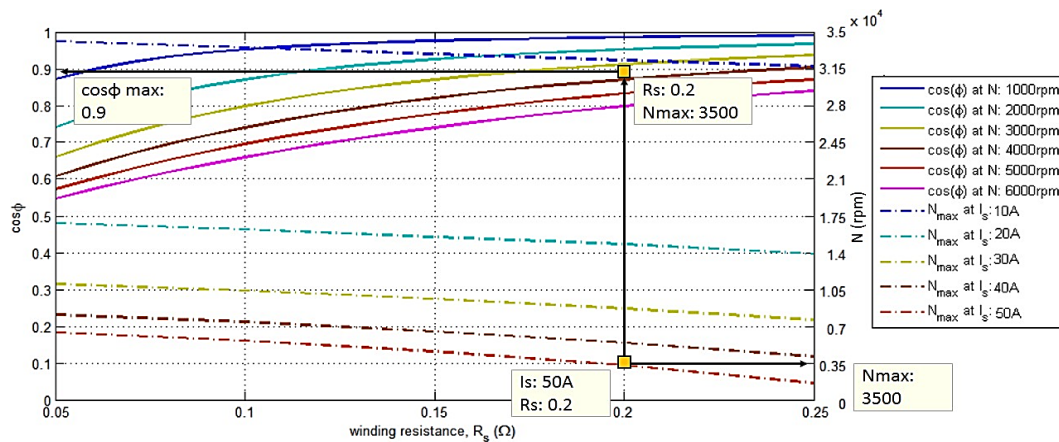


Figure 12. The abacus gives the speed limit at different current levels and power factor at different speeds as a function of winding resistance

On the right axis, the maximum speed for different currents (torque) can be found, plotted in dotted lines. The maximum speed was computed for a maximum voltage supply of 14 V. As the winding resistance increases, we can track the degradation of maximum speed for different current levels. On the left side, the reading of the axis gives the power factor at different speed levels, plotted in full lines.

With this graphical tool, a simple measurement of the winding resistance in real time can let us know the power factor and the maximum speed available for the machine. For example, for an operating point (T, N) of (0.57 N.m, 3500 rpm) where the current is at 50 A (from the reading of Figure 9), the winding resistance should not exceed 0.2Ω , or else, the speed will not be achievable. The maximum speed at this torque is indicated by the orange dotted lines. At the same time, if the winding resistance is at 0.2Ω , the power factor can be expected to be at around 0.9. This is an area between the yellow and brown full lines.

4. CONCLUSIONS AND PERSPECTIVES

In this study, an analytical model using the phasor diagram of the SynRM machine was built to identify the operating area and power factor. The computation using the tool has been validated on the prototype test bench. Using the validated model, the influence of temperature on the operating area and power factor was evaluated. We found that the maximum speed attainable by the machine is quadratically reduced with temperature increase. The power factor on the other hand is increased with the temperature. An abacus for maximum speed and power factor tracking was built following the findings to guide the user of the machine. Having the abacus for maximum speed and power factor tracking, a potential coupling between the thermal model previously developed with the abacus could further relate the motor utilization cycle to not only the winding temperature but also the power factor and operating area variation.

ACKNOWLEDGEMENTS




The authors would like to thank the Universiti Malaysia Pahang Al Sultan Abdullah for providing financial support under the internal grant RDU220302, the Ministry of Higher Education for the Fundamental Research Grant Scheme (FRGS) No. FRGS/1/2018/TK03/UMP/02/27 (University reference RDU190196), and the Séjour Scientifique Haut Niveau grant (SSHN) 952372C from the Ministry of Foreign Affairs of France managed by Campus France. We are also thankful for the facilities provided by both Universiti Malaysia Pahang and Université de Technologie de Compiègne.

REFERENCES




- [1] Z. Zhang, L. Wang, J. Zhang, and R. Ma, "Study on requirements for load emulation of the vehicle with an electric braking system," *IEEE Transactions on Vehicular Technology*, vol. 66, no. 11, pp. 9638–9653, 2017, doi: 10.1109/TVT.2017.2739425.
- [2] X. Yuan, Y. Wang, and L. Wu, "SVM-based approximate model control for electronic throttle valve," *IEEE Transactions on Vehicular Technology*, vol. 57, no. 5, pp. 2747–2756, 2008, doi: 10.1109/TVT.2008.917222.
- [3] M. A. H. Rasid, V. Lanfranchi, A. Ospina, and K. El Kadri Benkara, "Torque Ripple Analysis of Synchronous Reluctance Motor with Different Rotor Topologies for Application with Dimensional Constraint," *Journal of Electrical Engineering and Technology*, vol. 15, no. 5, pp. 2167–2177, 2020, doi: 10.1007/s42835-020-00493-8.
- [4] C. Doc, "Contribution à la Conception et au Dimensionnement d'un Actionneur d'Embrayage," *Université de Technologie de Compiègne, Laboratoire d'Electromecanique de Compiègne*, 2010.
- [5] M. A. H. Rasid, "Contribution to multi-physical studies of small synchronous-reluctance machine for automotive equipment," *Université de technologie de Compiègne*, 2016. doi: 10.13140/RG.2.1.5043.0960.
- [6] M. A. H. Rasid, A. Ospina, K. El Kadri Benkara, and V. Lanfranchi, "A thermal study on small synchronous reluctance machine in automotive cycle," in *2016 IEEE 25th International Symposium on Industrial Electronics (ISIE)*, Jun. 2016, pp. 134–140. doi: 10.1109/ISIE.2016.7744879.
- [7] B. Djamel, H. Houassine, N. Kabache, and D. Moussaoui, "Electromagnetic nonlinear parametric study of the SynRM using FEM method," *Indonesian Journal of Electrical Engineering and Computer Science*, vol. 24, no. 2, pp. 637–648, 2021, doi: 10.11591/ijeecs.v24.i2.pp637-648.
- [8] P. R. Viego, J. R. Gómez, V. Sousa, J. P. M. Yanes, and E. C. Quispe, "Reducing torque pulsations in pma-synrm: A way for improving motor performance," *International Journal of Power Electronics and Drive Systems*, vol. 12, no. 1, pp. 67–79, 2021, doi: 10.11591/ijpeds.v12.i1.pp67-79.
- [9] L. He, W. Shi, X. Xia, X. Wu, H. Chen, and X. Yan, "Research on Temperature Rise Characteristics of Vehicle Motors Under Bench Working Condition," *Journal of Electrical Engineering and Technology*, vol. 16, no. 6, pp. 3135–3143, 2021, doi: 10.1007/s42835-021-00853-y.
- [10] L. Cheng, Y. Kai, and W. Xiaoguang, "A design of high power factor single phase inverter," *2016 IEEE 8th International Power Electronics and Motion Control Conference, IPEMC-ECCE Asia 2016*, pp. 3111–3115, 2016, doi: 10.1109/IPEMC.2016.7512792.
- [11] N. Vazquez, J. Villegas-Saucillo, C. Hernandez, E. Rodriguez, and J. Arau, "Two-Stage Uninterruptible Power Supply With High Power Factor," *IEEE Transactions on Industrial Electronics*, vol. 55, no. 8, pp. 2954–2962, Aug. 2008, doi: 10.1109/TIE.2008.918475.
- [12] Y. Wang, D. Ionel, D. G. Dorrell, and S. Stretz, "Establishing the Power Factor Limitations for Synchronous Reluctance Machines," *IEEE Transactions on Magnetics*, vol. 51, no. 11, 2015, doi: 10.1109/TMAG.2015.2443713.
- [13] L. Huang, J. Feng, S. Guo, J. Shi, and Z. Q. Zhu, "Analysis of power factor in variable flux reluctance machines with MMF-permeance model," *IET Electric Power Applications*, vol. 13, no. 5, pp. 614–624, May 2019, doi: 10.1049/iet-epa.2018.5301.
- [14] H. Kim *et al.*, "A study on the rotor design of line start synchronous reluctance motor for ie4 efficiency and improving power factor," *Energies*, vol. 13, no. 21, p. 5774, Nov. 2020, doi: 10.3390/en13215774.
- [15] W. Pawlus, J. T. Birkeland, H. Van Khang, and M. R. Hansen, "Identification and Experimental Validation of an Induction Motor Thermal Model for Improved Drivetrain Design," *IEEE Transactions on Industry Applications*, vol. 53, no. 5, pp. 4288–4297, Sep. 2017, doi: 10.1109/TIA.2017.2700283.
- [16] S. W. Hwang, J. Y. Ryu, J. W. Chin, S. H. Park, D. K. Kim, and M. S. Lim, "Coupled Electromagnetic-Thermal Analysis for Predicting Traction Motor Characteristics According to Electric Vehicle Driving Cycle," *IEEE Transactions on Vehicular Technology*, vol. 70, no. 5, pp. 4262–4272, 2021, doi: 10.1109/TVT.2021.3071943.
- [17] K.-Y. Chen and R.-F. Fung, "Dynamic modelling and state observer-based robust control for a mechatronic system with temperature effect," *International Journal of Dynamics and Control*, vol. 9, no. 3, pp. 957–970, Sep. 2021, doi: 10.1007/s40435-021-00756-w.
- [18] S. Li, B. Sarlioglu, S. Jurkovic, N. R. Patel, and P. Savagian, "Analysis of Temperature Effects on Performance of Interior Permanent Magnet Machines for High Variable Temperature Applications," *IEEE Transactions on Industry Applications*, vol. 53, no. 5, pp. 4923–4933, Sep. 2017, doi: 10.1109/TIA.2017.2700473.
- [19] B. S. Gagas, K. Sasaki, A. Athavale, T. Kato, and R. D. Lorenz, "Magnet Temperature Effects on the Useful Properties of Variable Flux PM Synchronous Machines and a Mitigating Method for Magnetization Changes," *IEEE Transactions on Industry Applications*, vol. 53, no. 3, pp. 2189–2199, May 2017, doi: 10.1109/TIA.2017.2674627.
- [20] C. Lungoci and D. Stoia, "TEMPERATURE EFFECTS ON TORQUE PRODUCTION AND EFFICIENCY OF MOTORS WITH NdFeB," *Rev. Roum. Sci. Techn.-Électrotechn. et Énerg.*, vol. 53, pp. 445–454, 2008.
- [21] A. Ayachit and M. K. Kazmierczuk, "Thermal Effects on Inductor Winding Resistance at High Frequencies," *IEEE Magnetics Letters*, vol. 4, pp. 0500304–0500304, 2013, doi: 10.1109/LMAG.2013.2286582.
- [22] I. Boldea, "Reluctance synchronous machines and drives," *Clarendon Press*, vol. 38, 1996.
- [23] M. A. H. Rasid, K. Benkara, and V. Lanfranchi, "Fast electro-mechanical performance evaluation tool for synchronous reluctance machine," *International Journal of Precision Engineering and Manufacturing*, vol. 18, no. 11, pp. 1567–1573, Nov. 2017, doi: 10.1007/s12541-017-0186-1.
- [24] N. Bianchi, "Electrical machine analysis using finite elements," *Electrical Machine Analysis Using Finite Elements*, pp. 1–275, 2017, doi: 10.1201/9781315219295.
- [25] A. Accetta, M. Cirrincione, M. C. Di Piazza, G. La Tona, M. Luna, and M. Pucci, "Analytical Formulation of a Maximum Torque per Ampere (MTPA) Technique for SynRMs Considering the Magnetic Saturation," in *2019 IEEE Energy Conversion Congress and Exposition (ECCE)*, Sep. 2019, pp. 4024–4029. doi: 10.1109/ECCE.2019.8912653.

BIOGRAPHIES OF AUTHORS






Mohd Azri Hizami Rasid    received his Ph.D. degree in mechatronics from Université de Technologie de Compiègne, France in 2016. He is also an IEEE Senior member. He is currently a senior lecturer in the Faculty of Manufacturing and Mechatronics Engineering Technology, Universiti Malaysia Pahang. He is a researcher belonging to the Mechatronics Systems and Design Research Group. His research focuses on electromechanical systems with multiphysic approach, focusing on thermal and vibro-acoustic behavior. His teaching areas include electrical engineering, mechatronics, and controls. He can be contacted at email: mahizami@ump.edu.my.






Vincent Lanfranchi    received his Ph.D. degree in electrical engineering from the University of Reims (France) in 2000. He is now a full professor at the Université de Technologie de Compiègne. His teaching areas are electrical engineering and mechatronics. He was a researcher in the LEC laboratory (Laboratoire d'Electromecanique de Compiègne) from 2001 to 2017. He is now head of M2EI (mechatronic, energy, electricity, integration) team in the ROBERVAL Laboratory at UTC. His main research interest is the design of electromechanical systems for energy conversion with multi-physic approach. It also focuses on harmonic behavior including converter-machine interactions and Pulse Width Modulation strategies. He can be contacted at email: vincent.lanfranchi@utc.fr.



Alejandro Ospina    received his Ph.D. degree in applied physics from the Université de Paris Sud (France) in 2010. He is now an associate professor at the Université de Technologie de Compiègne. His teaching areas are electrical engineering and mechatronics. He was a researcher in the LEC laboratory (Laboratoire d'Electromecanique de Compiègne) from 2001 to 2017. He is now a member of M2EI (mechatronic, energy, electricity, integration) team in the ROBERVAL Laboratory at UTC. His main research interest includes studies of magnetic materials using additive manufacturing, thermal instrumentation and analysis for electrical machines. He can be contacted at email: alejandro.ospina@utc.fr.



Khadija Benkara    received the Dipl.-Eng. degree in electrical engineering from the Ecole Nationale Supérieure d'Electrotechnique, d'Electronique, d'Informatique, et d'Hydraulique de Toulouse (ENSEEIH), Toulouse, France, in 1998, and the Ph.D. degree in engineering sciences from the University of Technology of Belfort-Montbéliard, Belfort, France, and University of Besançon, Besançon, France, in 2006. She is currently a Research Engineer with the Roberval Laboratory, University of Compiègne, Compiègne, France. His main research activities concern multiphysic modeling of electric actuators and energy sources and application to electric/hybrid vehicles. She can be contacted at email: khadija.el-kadri-benkara@utc.fr.